Films of Non-Newtonian Fluids Adhering to Flat Plates

CHAIM GUTFINGER and JOHN A. TALLMADGE

Yale University, New Haven, Connecticut

This paper presents a study of flux, film thickness, and velocity profiles in the drainage and withdrawal processes of non-Newtonian fluids on flat plates. The flow equations for the drainage from a vertical plate are solved for a three-constant or Ellis model fluid. The solution is compared with that of the Newtonian fluid.

The withdrawal case is solved for the power law fluid. The solution consists of matching of the equation of capillary statics in the liquid bath to the flow equation in the entrained film. Experimental data of coating of an endless belt with a film of a non-Newtonian fluid are presented and discussed in view of the theory developed.

When a flat plate is withdrawn from a liquid bath, a liquid film will adhere to it. Knowledge of the thickness of this film and the amount of liquid withdrawn (the flux) are important to many practical applications, some examples of which are coating of photographic films (*2*), metal coating (hot tinning, enamelling, etc.), and lubrication of moving machine parts (*1*). Another example requiring the knowledge of fluid dynamics of liquid films is the drainage of paints after deposition on a vertical support during painting.

In many cases, the fluids involved in drainage and withdrawal operations are non-Newtonian. Although the equivalent Newtonian case has been studied extensively, both theoretically (*2, 10, 16*) and experimentally (*2, 12, 15*), the results cannot, in general, be applied to non-Newtonian fluids. This article presents the results of a study for non-Newtonian fluids. Both drainage and withdrawal cases are considered theoretically. Experiments are reported for the withdrawal case only.

For this analysis, the fluids were assumed to be simple non-Newtonian fluids without elastic properties or memory. In the drainage case, the fluid used in the theoretical description was the three-constant Ellis model. For the withdrawal case, the power law fluid was employed. Although the influence of elastic properties was not investigated theoretically, a viscoelastic fluid [carboxymethyl cellulose (CMC) solution] was tested. This test was made to estimate deviations both from the simple theory and from the experiments with inelastic fluids, such as aqueous Carbopol solutions.

ASSUMPTIONS

The discussion presented here is limited to laminar films which are stable, that is without waves or ripples on the surface. The stability limitation is less serious for the case of non-Newtonian fluids that are by nature more viscous than for the Newtonian ones. Inertia forces are assumed to be negligible (*7*). In addition, it is assumed that the velocity in the direction normal to the plate is negligible compared with the velocity parallel to the plate; the resultant problem is thus simplified to a one-dimensional flow model. However, as in the case of boundary-layer solutions, these assumptions must be justified, either by experimental evidence or by analysis of the solution a posteriori.

Chaim Gutfinger is with Allied Chemical Corporation, Morristown, New Jersey.

FORMULATION OF THE PROBLEM

Using the assumptions made above, Levich (*10*) and Deryagin (*2*) arrived at a flow equation which can be generalized for a broader class of fluids as follows:

$$0 = \frac{1}{\rho}\frac{\delta \tau_{xy}}{\delta y} + g + \frac{\sigma}{\rho}\frac{d^3h}{dx^3} \qquad (1)$$

These three terms represent the viscous, gravitational, and surface tension effects, respectively.

Equation (1) holds both for drainage and withdrawal. In fact, by a proper transformation of coordinates, one can substitute one case for the other. In the case of withdrawal, the lower edge of the plate is always immersed in the liquid bath; however, for drainage, the plate can be either immersed or unimmersed. For the immersed case, the thickness of the liquid film near the bottom of the plate changes from a small value to infinity. Thus, in this region, the radius of curvature and the effect of surface

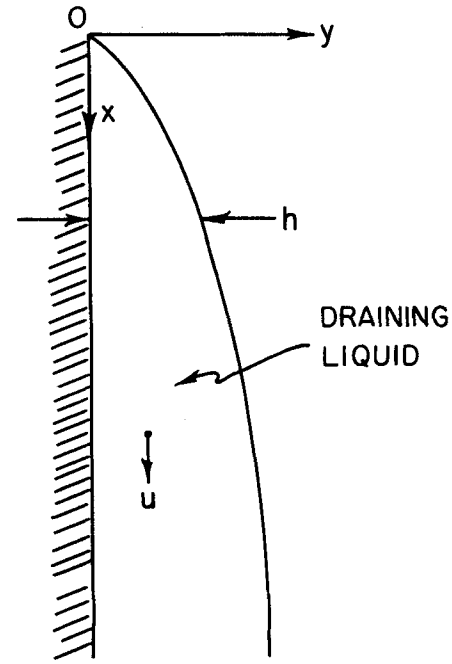

Fig. 1. Sketch of draining liquid.

tension change appreciably. In the case of unimmersed drainage, the change in thickness is finite and not large, suggesting that surface tension effects may be neglected for this situation. Experimental data confirm this assumption for Newtonian fluids (*14*). In the case of non-Newtonian fluids where viscous forces are generally higher, this assumption is expected to hold even better.

In the following discussion, the unimmersed type will be referred to as *drainage*. As the flow equation for this case does not contain the surface tension term, it can be solved for a more complex stress vs. rate-of-strain relationship.

THE DRAINAGE CASE

The flow equation for this case is

$$0 = \frac{1}{\rho}\frac{\delta \tau_{xy}}{\delta y} + g \tag{2}$$

with the y coordinate normal to and x parallel to the plate (Figure 1). The boundary conditions for this case are

$$u = 0 \text{ at } y = 0 \tag{3}$$

$$\tau_{xy} = 0 \text{ at } y = h \tag{4}$$

The fluid used here will be the one defined by the so-called Ellis model

$$\frac{\delta u}{\delta y} = \tau_{xy}\left[a + b\left|\tau_{xy}\right|^{s-1}\right] \tag{5}$$

which includes as special cases the power-law fluid when $a = 0$, the Newtonian fluid for $b = 0$, and the two regimes of the Bingham plastic fluid, that for $s = 0$ and that for $a = b = 0$.

Equations (5) and (2) can be combined and integrated twice with the two boundary conditions to yield the velocity profile across the film:

$$u = a\rho g\left(hy - \frac{1}{2}y^2\right) + \frac{b(\rho g)^s}{s+1}\left[h^{s+1} - (h-y)^{s+1}\right] \tag{6}$$

From this, the velocity at the air liquid interface is

$$u_h = \frac{1}{2}a\rho g h^2 + \frac{b(\rho g)^s}{s+1}h^{s+1} \tag{7}$$

and the flow rate per unit width of plate for a film of thickness h is

$$Q = \int_0^h u dy = a\rho g\frac{h^3}{3} + b(\rho g)^s\frac{h^{s+2}}{s+2} \tag{8}$$

Applying the continuity concept (*15*) to this case and combining with Equation (8), one gets

$$-\frac{\delta h}{\delta t} = \left[a\rho g h^2 + b(\rho g)^s h^{s+1}\right]\frac{\delta h}{\delta x} \tag{9}$$

Equation (9), solved with the initial condition $h(0, t) = 0$, yields an implicit relationship in h:

$$x = \left[a\rho g h^2 + b(\rho g)^s h^{s+1}\right]t \tag{10}$$

The amount of fluid on a plate of length x is also of interest. This can be obtained by defining a mean thickness $\overline{h}$ by

$$\overline{h} = \frac{1}{x}\int_0^x h dx \tag{11}$$

Differentiating Equation (10) for dx, substituting together with x into Equation (11), and integrating, one obtains the mean thickness for a plate of length x in terms of fluid properties and the point thickness at x:

$$\overline{h} = \frac{\frac{2}{3}a\rho g h + \frac{s+1}{s+2}b(\rho g)^s h^s}{a\rho g + b(\rho g)^s h^{s-1}} \tag{12}$$

This relationship, between $\overline{h}$ and h, provides an indication of the uniformity of the liquid coating.

By a similar procedure, but with two equations used to describe fluid behavior, the Q, $\overline{h}$, and h relationships for a Bingham plastic fluid have also been derived (*8*).

SPECIAL CASES OF DRAINAGE

For the case of a Newtonian fluid ($a = 1/\mu$, $b = 0$), Equations (8), (10), and (12) yield the solution determined by Jeffreys (*9*).

A power law fluid is defined by the model

$$\tau_{xy} = K\left|\frac{\delta u}{\delta y}\right|^{n-1}\frac{\delta u}{\delta y} \tag{13}$$

Thus $a = 0$, $b = 1/K^s$, and $s = 1/n$. For this type of fluid, Equations (8), (10), and (12) reduce to

$$Q = \frac{n}{2n+1}\left(\frac{\rho g}{K}\right)^{\frac{1}{n}}h^{\frac{2n+1}{n}} \tag{14}$$

$$h = \left(\frac{K}{\rho g}\right)^{\frac{1}{n+1}}\left(\frac{x}{t}\right)^{\frac{n}{n+1}} \tag{15}$$

$$\overline{h} = \frac{n+1}{2n+1}h \tag{16}$$

These equations for power law fluids reduce to those for Newtonian fluids when $n = 1$, at which time $K = 1/\mu$.

With Equations (14), (15), and (16), the effects of various parameters on the film thickness were compared for the two special cases listed above. Some conclusions based on these comparisons are listed below for power law fluids of $0 < n < 1$.

1. The change of the viscosity coefficient K in the power law case will have a more pronounced influence on the thickness than the change in viscosity coefficient μ in the Newtonian case, see Equation (15).
2. The change of thickness with time and place is more pronounced in the Newtonian case than in the power law one, see Equation (15).
3. The flow rate is a stronger function of the thickness in the Newtonian case than in the power law case, see Equation (14).
4. The power law liquid film is of a more uniform nature than the Newtonian one, see Equation (16) for mean thickness.
5. The above mentioned effects become more apparent with decreasing n.

The solution presented in this part is also applicable for a special case of withdrawal where viscous forces are much larger than surface tension forces. This occurs at the higher speed withdrawals. In order to be able to use the above equations, one has to substitute u_o, the withdrawal speed, in place of the group (x/t). This application is described subsequently in the development of Equation (46).

The importance of drainage theory for withdrawal studies is discussed further in the last few paragraphs before the Summary.

THE WITHDRAWAL CASE

The continuous withdrawal process can be described conveniently by subdividing it into three regions (Figure 2).

1. The region well above the liquid level. In this region, the film thickness h_o is constant with respect to height, as shown experimentally (*8, 15*); thus all the derivatives of thickness with respect to the distance x are equal to zero here. As shown by Laplace's equation for surface tension, pressure changes due to surface tension require curved surfaces; because of the flat surface, surface tension effects do not enter the flow equation for this region. These conditions have been discussed in detail elsewhere (*10*).

2. This is the region of the dynamic meniscus. Here h changes with distance, and all three forces constituting Equation (1) are present.

3. This is the region close to the water line. Here the flow effects are less pronounced, and the system can be described by the equation of capillary statics.

A proper matching of these three regions into a combined solution will provide the answer to this problem. It should be emphasized that, because of the approximate nature of both the subdivision and the matching procedure, one does not expect to be able to determine the solution for the true thickness profile. However, it is sufficient for practical purposes if the ultimate steady state thickness h_o is known as a function of withdrawal speed and fluid properties, provided that the transition region of the dynamic meniscus is not too large. The flow equations for the different regions are the following:

1.

$$0 = \frac{1}{\rho}\frac{\delta \tau_{xy}}{\delta y} + g \tag{17}$$

2.

$$0 = \frac{1}{\rho}\frac{\delta \tau_{xy}}{\delta y} + g + \frac{\sigma}{\rho}\frac{d^3h}{dx^3} \tag{18}$$

3.

$$\frac{\dfrac{d^2h}{dx^2}}{\left[1 + \left(\dfrac{dh}{dx}\right)^2\right]^{3/2}} = \frac{\rho g x}{\sigma} \tag{19}$$

The boundary conditions for the moving film are

$$u = u_o \quad \text{at} \quad y = 0 \tag{20}$$

$$\tau_{xy} = 0 \quad \text{at} \quad y = h \tag{21}$$

where u_o is the withdrawal speed of the solid support. Regions 1 and 2 can be matched together by using the steady state condition of equal flow rates in both regions

$$Q_1 = Q_2 \tag{22}$$

The free constant for matching is h_o. Equations (17) and (18) are integrated for the power law fluid, Equation (13) to obtain the flow rates. The integrating procedure is similar to the one used in the drainage case. The results are substituted into Equation (22) to yield

$$u_o h_o - \frac{n}{2n+1}\left(\frac{\rho g}{K}\right)^{\frac{1}{n}} h_o^{\frac{2n+1}{n}} = u_o h - \frac{n}{2n+1}\left(\frac{\rho g}{K} + \frac{\sigma}{K}\frac{d^3h}{dx^3}\right)^{\frac{1}{n}} h^{\frac{2n+1}{n}} \tag{23}$$

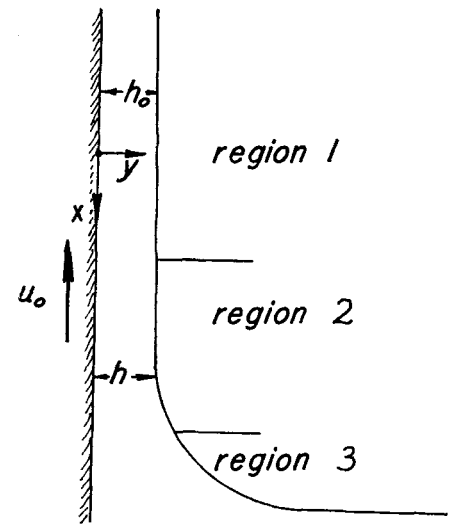

Fig. 2. Diagram of the withdrawal process.

This equation is a third-order differential equation in h. The boundary conditions are taken at the juncture of Regions 1 and 2; as discussed above, all derivatives of h with x vanish in Region 1. Thus the boundary conditions are

$$h = h_o, \quad \frac{dh}{dx} = 0, \quad \frac{d^2h}{dx^2} = 0 \text{ at } x = x_o \tag{24}$$

Because Equation (23) does not contain x, x_o may be defined relative to any chosen place so that it will determine the edge of Region 1. It is convenient to set $x_o = 0$. Equation (18), combined with Equation (17) by means of Equation (22), yields Equation (23). Equation (23) has been solved numerically, and the solution will be described forthwith. However, it should be noted that the solution of this equation is not sufficient to specify h_o as a function of withdraw speed and fluid properties; this insufficiency has been discussed for Newtonian fluids (*10*). The other condition necessary to specify h_o may be provided by Region 3; for this reason the matching equation of capillary statics was used in this work.

Equation (23) can be put in dimensionless form by defining the following dimensionless groups:

Dimensionless thickness:

$$T = h\left(\frac{\rho g}{K u_o^n}\right)^{\frac{1}{n+1}} \tag{25}$$

Dimensionless withdrawal speed, capillary number, the ratio between viscous force and surface tension:

$$N_{Ca} = \frac{K}{\sigma} h_o^{1-n} u_o^n \tag{26}$$

The dependent variable—relative thickness:

$$L = \frac{h}{h_o} \tag{27}$$

Independent variable—dimensionless coordinate:

$$\lambda = \left[\left(\frac{2n+1}{n}\right)^n \frac{K}{\sigma}\frac{u_o^n}{h_o^{n+2}}\right]^{\frac{1}{3}} x \tag{28}$$

Or, alternately:

$$\lambda = \left[\left(\frac{2n+1}{n}\right)^n N_{Ca}\right]^{\frac{1}{3}} \frac{x}{h_o} \tag{29}$$

Combining Equations (25) to (28) with Equation (23) one obtains, where T_o refers to h_o

$$\frac{d^3L}{d\lambda^3} = \left(\frac{n}{2n+1}\right)^n T_o^{n+1} - \frac{\left(L - 1 + \frac{n}{2n+1} T_o^{\frac{n+1}{n}}\right)^n}{L^{2n+1}} \tag{30}$$

with the boundary conditions

$$L = 1,\ L' = 0,\ L'' = 0 \text{ at } \lambda = 0 \tag{31}$$

Now going back to the equation of capillary statics, Equation (19), and integrating it once with the boundary condition $h \to \infty$ at the water line, one obtains similarly to Levich (*10*)

$$\frac{\frac{dh}{dx}}{\left[1 + \left(\frac{dh}{dx}\right)^2\right]^{1/2}} = \frac{\rho g x^2}{2\sigma} - 1 \tag{32}$$

Using the condition that $dh/dx \to 0$ as $h \to h_o$, together with Equations (32) and (19), one arrives at

$$\left(\frac{d^2h}{dx^2}\right)_{h \to h_o} \to \sqrt{2}\left(\frac{\rho g}{\sigma}\right)^{1/2} \tag{33}$$

which is, in dimensionless coordinates

$$\left(\frac{d^2L}{d\lambda^2}\right)_{L_3 \to 1} \to \frac{\sqrt{2}}{h_o}\left(\frac{\rho g}{\sigma}\right)^{\frac{1}{2}} \left[\left(\frac{n}{2n+1}\right)^n \frac{\sigma h_o^{n+2}}{K u_o^n}\right]^{\frac{2}{3}} \tag{34}$$

In order to match the solution for the static meniscus (Region 3) with that of the flow equation (Region 2), one has to fulfill the condition that, somewhere in the film, there is a region where the curvature computed from the dynamic equation is identical to the one computed from the static equation. Physically, this means that the computed solution gives an unbroken surface, whether it is approached from the dynamic equation's side or from that of the static meniscus. This matching region is in the range of thickness that is large compared with the limiting thickness h_o, but at the same time small compared with the film thickness in the static meniscus region.

The matching condition of equal radii of curvature (*10*) can be stated in dimensionless form as

$$\left(\frac{d^2L}{d\lambda^2}\right)_{L_2 \to \infty} = \left(\frac{d^2L}{d\lambda^2}\right)_{L_3 \to 1} \tag{35}$$

The right-hand side of Equation (35) is given by Equation (34), while the left side is found by integrating Equation (30). The success of this integration depends on the rate at which the second derivative $(d^2L/d\lambda^2)$ converges as $L \to \infty$. From Equation (30) it is apparent that the third derivative approaches a constant as $L \to \infty$ for any nonvanishing T_o; thus, the second derivative will not converge for nonvanishing T_o. Only for the case where $T_o \to 0$ will the third derivative vanish as $L \to \infty$; for this special case of small values of T_o, the second derivative will approach a constant α. Thus:

$$\left(\frac{d^2L}{d\lambda^2}\right)_{L_2 \to \infty} = \alpha \quad \text{for} \quad T_o \to 0 \tag{36}$$

In order to obtain α for various values of n, one has to solve the following third-order nonlinear differential equation, obtained by letting $T_o = 0$ in Equation (30):

$$\frac{d^3L}{d\lambda^3} = -\frac{(L-1)^n}{L^{2n+1}} \tag{37}$$

Once α is obtained, it can be substituted into Equation (34), thus providing a relationship for h_o as a function of speed of withdrawal and fluid properties for the case of small values of T_o.

Equation (37) was solved numerically on an IBM-709 digital computer. A modified Euler method employing the slopes in the middle of each interval was used. Solutions were obtained for nine values of n from 0.2 to 1.0. In order to save computer time without losing accuracy, a variable step of integration was employed. The solution is quite sensitive to the step size at the starting point near $L = 1$. Later, however, when L becomes large, the third derivative doesn't change much. Therefore, a small initial step Δ was used, which was increased after each computation in accordance with the following scheme:

$$\Delta_{i+1} = 1.01\,\Delta_i \tag{38}$$

The values of α obtained from the solution are tabulated in Table 1. These values can be expressed by an equation that fits the data with an accuracy of better than 2% in α:

$$\alpha = 0.646 - 0.76 \ln n \tag{39}$$

Thus, for the case of small T_o, the equation expressing the thickness as a function of speed of withdrawal and fluid properties is as follows:

$$h_o = \left[\left(\frac{2n+1}{n}\right)^{2n} \left(\frac{\alpha}{\sqrt{2}}\right)^3 \frac{K^2 u_o^{2n}}{\sqrt{\sigma}\,(\rho g)^{3/2}}\right]^{\frac{1}{2n+1}} \tag{40}$$

this is, in dimensionless form

$$T_o = \left[\frac{\alpha^2}{2}\left(\frac{2n+1}{n}\right)^{\frac{4n}{3}} N_{Ca}^{\frac{1}{3}}\right]^{\frac{1}{n+1}} \tag{41}$$

One can also define a mean thickness as

$$\bar{h} = \frac{Q}{u_o} \tag{42}$$

which yields upon substitution of Q from the left-hand side of Equation (23):

Table 1. The Effect of n on α
[See Equations (36) and (41)]

n	α	n	α
0.2	1.742	0.7	0.910
0.3	1.514	0.8	0.809
0.4	1.324	0.9	0.720
0.5	1.164	1.0	0.643
0.6	1.028		

Table 2. The Effect of n on β
[See Equations (51) and (52)]

n	β	n	β
0.2	30.5	0.7	0.987
0.3	4.41	0.8	0.837
0.4	2.27	0.9	0.727
0.5	1.56	1.0	0.643
0.6	1.21		

$$\bar{h} = h_o \left[1 - \frac{n}{2n+1} \frac{h_o}{u_o}^{\frac{n+1}{n}} \left(\frac{\rho g}{K}\right)^{\frac{1}{n}} \right] \quad (43)$$

This can be put in dimensionless form as

$$\bar{T} = T_o \left[1 - \frac{}{2n+1} T_o^{\,n+1} \right] \quad (44)$$

The physical meaning of $\bar{h}$ is the thickness the liquid film would have had if the whole film had moved upward with a velocity u_o. This is also the thickness of the film after it solidifies, as is the case in coating of photographic films. It is the feeling of the authors that this quantity $\bar{h}$ is a more important one practically than h_o.

The solution presented above is for the case of small values of T_o; as shown by Equation (41), this implies small capillary numbers or relatively small withdrawal speeds. On the other hand for the case of large capillary numbers, that is, the case where viscous forces are very large as compared with surface tension, the solution can be adapted from the drainage case by substituting u_o for (x/t) in Equation (15) as stated above. This yields

$$h_o = \left(\frac{K u_o^n}{\rho g} \right)^{\frac{1}{n+1}} \quad (45)$$

or in dimensionless form

$$T_o = 1 \quad (46)$$

$\bar{T}$ can be computed either from Equation (16) or (44) to yield

$$\bar{T} = \frac{n+1}{2n+1} \quad (47)$$

THE MORE GENERAL SOLUTION

The equations presented above are expected to hold in the regions of small T_o ($T_o \to 0$) or in large T_o ($T_o \to 1$), or in other words, for low N_{Ca} or high N_{Ca}. However, one can also solve Equation (30) approximately for the case of any T_o. Let $L = 1 + \epsilon$, where ϵ is a small number. Equation (30) can then be written as

$$\frac{d^3\epsilon}{d\lambda^3} = \frac{\left(\frac{n}{2n+1}\right)^n T_o^{n-1}(1+\epsilon)^{2n+1} - \left(\frac{n}{2n+1} T_o^{\frac{n+1}{n}} + \epsilon\right)^n}{(1+\epsilon)^{2n+1}} \quad (48)$$

Expanding the two binomials into Taylor series, truncating after the second term and performing the appropriate algebraic operations, one arrives at

$$\frac{d^3\epsilon}{d\lambda^3} = \frac{n^n}{(2n+1)^{n-1}} T_o^{n+1}\left(1 - T_o^{-\frac{n+1}{n}}\right) \frac{\epsilon}{(1+\epsilon)^{2n+1}} \quad (49)$$

Defining a new independent variable

$$\chi = \left[n^n (2n+1)^{1-n} T_o^{n+1} \left(1 - T_o^{-\frac{n+1}{n}}\right) \right]^{\frac{1}{3}} \lambda \quad (50)$$

and returning to L notation, one obtains

$$\frac{d^3L}{d\chi^3} = -\frac{L-1}{L^{2n+1}} \quad (51)$$

Equation (51) was integrated numerically in a similar way to Equation (37), yielding the values of $\beta =$ shown in Table 2.

The relationship for evaluation of T_o is, in dimensionless form

$$N_{Ca} = \frac{8}{\beta^6 (2n+1)^4} \frac{T_o^{\frac{(4-n)(n+1)}{n+1}}}{\left(1 - T_o^{\frac{n}{n+1}}\right)^4} \quad (52)$$

Where $n = 1$, Equation (52) reduces to the Newtonian solution of White and Tallmadge (*16*). This Newtonian solution agreed with actual data for Newtonian fluids within experimental precision; it was found to be better than the Newtonian equivalent of Equations (41) and (46) for the region of capillary number from about 0.03 up to the highest N_{Ca} previously reported (*15*), which was about $N_{Ca} = 3$.

EXPERIMENTAL

The experimental apparatus, similar to that of Van Rossum (*15*), is shown in Figure 3. The infinitely long plate consisted of an endless stainless steel belt 250 cm. long and 6.5 cm. wide, made by carefully welding together the ends of 250 cm. long sheet. The joint was ground until it attained the thickness of the belt, which was 0.015 cm. Thickness variation was less than 0.0005 cm., except at the joint where the thickness was allowed to be 0.001 cm. less than the rest of the belt.

The belt was positioned between two pulleys where it was tightened and leveled by means of a screw mechanism on one of the pulleys. The belt was driven at speeds from 0.35 to 82.2 cm./sec. by means of a thyratron controlled motor with a potentiometer used for speed selection. The motor was connected through a flexible coupling to the upper pulley, but the pulley assembly and the motor were kept on two independent supports in order to eliminate vibrations. The lower pulley was immersed in the liquid bath. When the belt was moved, the liquid was entrained on the belt and a liquid film was formed.

The film thickness h_o or T_o was measured directly at the center of the belt by means of a micrometric screw built perpendicular to a small pulley which was pressed toward the belt. Two ways of indicating the touching point were used. With a conducting, aqueous solution, this point was indicated on a galvanometer by the closing of an electrical circuit through the liquid. For nonconducting fluids, the touching point was determined visually, a technique that was surprisingly reproducible and precise. The zero calibration was

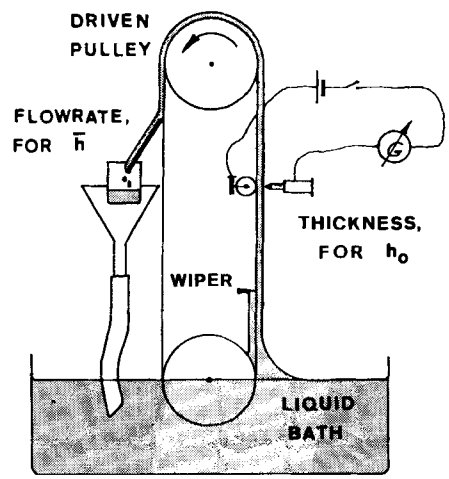

Fig. 3. Apparatus for continuous withdrawal (schematic).

measured on the moving belt without the fluid by the electric circuit method.

Each thickness was measured five to ten times. The average variation of the different measurements at a given set of conditions was about ± 0.003 cm. This results in a possible error of as much as ± 30% for the lowest thicknesses measured, being around 0.01 cm., and as low as ± 1% for the highest thicknesses, which were around 0.3 cm. On the average, the accuracy of the thickness measurements is estimated at ± 3%. No variation in thickness with height was noted from 30 to 100 cm. above the bath. Slight wave formation occurred at high withdrawal speeds with Newtonian fluids; for these cases no data were taken.

As an independent check, the flow rate was determined by weighing the mass of liquid wiped from the belt during a measured time interval, An automobile windshield wiper blade was used for wiping. Flow rates were expressed as mean thicknesses $\overline{h}$ by Equation (42). Film thicknesses and flow rates were converted to a common basis for comparison by use of Equation (43). Each flow rate was measured three times. On the average, the accuracy of the measurements was about ± 3%. Slight differences in film thicknesses were observed at the edges of the belt; but as these were minor, flow rate measurements were not affected.

In addition, withdrawal experiments were performed with finite plates on one Newtonian and one non-Newtonian fluid. The same experimental setup was used as in the continuous withdrawal, except the plate was attached to the upper pulley and withdrawn at each speed from several immersion depths. The mean thickness $\overline{h}$ (and $\overline{T}$) was determined from the measured adhering mass by dividing by the immersed area and fluid density. The small end effects were eliminated by plotting the mean thickness vs. the reciprocal of immersed depth ($1/d$) and extrapolating to $1/d = 0$. This technique has been previously used by Morey (*12*) and Van Rossum (*15*). Each mass measurement was repeated three to five times; the estimated precision of these finite plate mean thicknesses is about ± 4%.

Viscosities of Newtonian fluids were determined by means of ASTM calibrated capillary viscometers. The flow curves for non-Newtonian fluids were determined from measurements in a concentric cylinder viscometer, modified by redesigning the inner cylinders to a shape in which end effects have been minimized, providing a jacket for the outer cylinder through which water from a constant temperature bath was circulated, and calibrating the viscometer tension spring. The rheological constants K and n were determined by means of a computer program utilizing a least-square technique.

Surface tension measurements were performed for the less viscous Newtonian fluids by measuring the rise of the liquid in a capillary. For the more viscous Newtonian as well as all the non-Newtonian fluids, the measurements were performed by means of a ring tensiometer.

More detailed descriptions of apparatus, measuring techniques, computer programs, and calibration procedures can be found elsewhere (*8*).

EXPERIMENTS WITH NEWTONIAN FLUIDS

Newtonian experiments were performed in order to check the equipment and to compare the data with the literature (*3, 10, 16*). Three types of measurements were performed for comparison: film thickness and flow rate measurements for continuous withdrawal and finite plate measurements of mean thickness. The properties of the Newtonian fluids used along with the type of experiments performed are listed in Table 3.

For reasons of comparison with non-Newtonian fluids, film thickness results are presented both as plots of h_o vs. $u_o^{2n/2n+1}$ and of $\overline{T}$ vs. N_{Ca}. For non-Newtonian results, the first form was primarily intended to compare the speed dependence predicted by theory with that found experimentally (showing agreement with theory), and the second form was primarily intended to compare the magnitude of the predicted film thickness with measured values (showing disagreement with theory).

TABLE 3. PROPERTIES OF NEWTONIAN FLUIDS TESTED

Fluid no.	Description	Measurements	Density, g./cc.	Viscosity, poise	Surface tension, dynes/cm.
1.	Glycerine	Thickness	1.259	5.99	59.0
2.	Glycerine-water	Thickness	1.254	4.92	60.0
3.	Glycerine-water	Thickness, flow rate	1.220	1.03	52.5
4.	Glycerine-water	Thickness	1.202	0.472	62.5
5.	Mineral oil	Thickness, flow rate	0.880	1.60	31.7
6.	Glycerine	Finite plate	1.259	6.18	59.0

The $h_o - u_o$ plots on Figures 4 and 6 indicate the thickness data and the speeds used in directly measured form, together with separate lines for each fluid; thus, these plots served to replace tabulations of conditions studied. The $h_o - u_o$ plots were also used for developing the numerical coefficient in the final correlation. The $\overline{T} - N_{Ca}$ plots tend to draw the data together to general relationships over a range of fluid properties; however, they have dimensionless groups whose implications may not be readily apparent to those unfamiliar with withdrawal design.

As shown in Figure 4, the measured film thickness for fluids 1 to 5 were plotted vs. $u_o^{2/3}$ in accordance with the simplified theory of Equation (41). The resultant straight-line relationships on this plot indicate that the effect of u_o predicted by Equation (41) was followed closely over the thirty-fold speed range covered and over the range of fluid properties studied.

The data for all three types of measurements and all Newtonian fluids are shown in a $\overline{T}$ vs. N_{Ca} plot in Figure 5, along with three theoretical Equations (41, 46, 52). Values of $\overline{T}$ were calculated from Equation (44) for all these equations and for the film thickness data. Comparison of film thickness of fluid number 1 with finite plate data for fluid number 6 and comparison of thickness with flow rates for both fluids number 3 and number 5 indicate agreement of the three types of measurement, within experimental precision.

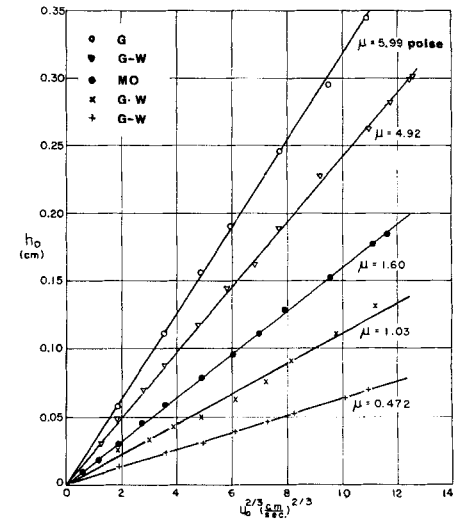

Fig. 4. Effect of withdrawal speed on film thickness—Newtonian fluids ($n = 1$).
G = glycerine
GW = glycerine-water solutions
MO = mineral oil

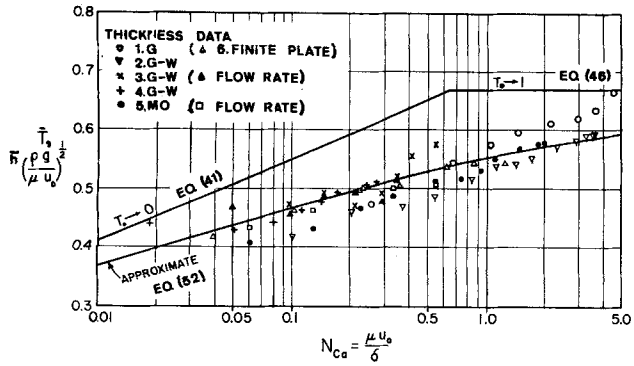

Fig. 5. Effect of capillary number on dimensionless mean thickness—Newtonian fluids ($n = 1$).

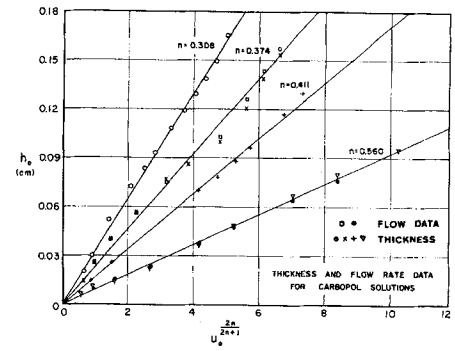

Fig. 6. Effect of withdrawal speed on film thickness—power law fluids ($n < 1$).

Taken together, the data for the various fluids fall in the same general area, indicating that the theory predicts the effect of fluid properties satisfactorily. The spread of the data, which was about ± 10%, is somewhat larger than the maximum possible experimental error of about ± 5%. This considerable spread is apparently due to a second-order effect which is not fully understood. Similar discrepancies can be observed in experimental data appearing in the literature (3).

Of all the theoretical equations, Equation (52) predicts the magnitude of mean film thickness best, as indicated previously with other data (16). The $\overline{T}$ values calculated from the simplified theory, Equations (41) and (46), are slightly higher than those obtained by experiment; this difference can be understood by examining the assumptions on which the theory is based.

Equation (41) was obtained by matching the dynamic equation in Region 2 with static meniscus equation in Region 3. However, the matching was not done at the same point (equal L) but rather at two different values of L (∞ and 1), as seen from Equation (35):

$$(d^2L/d\lambda^2)_{L_2 \to \infty} = (d^2L/d\lambda^2)_{L_3 \to 1} \qquad (35)$$

For Region 2 this derivative at $L_2 \to \infty$ is the maximum value in the whole region, while for Region 3 the derivative at $L_3 \to 1$ is the minimum value in the static meniscus region. Both contribute to the increase of the value of T_0 (or $\overline{T}$) for a given N_{Ca}. Thus $\overline{T}$ values predicted from Equation (41) are conservative; they indicate the upper limit rather than the average value of the data. On the other hand, Equation (52), which was developed from similar matching conditions for a more general equation, correlates experimental data quite well. This is a rather successful coincidence.

Table 4. Properties of Non-Newtonian Fluids Used in Experiments

Fluid no.	Aqueous solutions, mass %	Measurements	Power law constants K	Power law constants n	Density, g./cc.	Surface tension, dynes/cm.
7.	0.16% Carbopol	Thickness, flow rate	6.01	0.56	1.00	57.7
8.	0.18% Carbopol	Thickness	22.6	0.412	1.00	64.2
9.	0.19% Carbopol	Thickness, flow rate	34.4	0.374	1.00	70.5
10.	0.20% Carbopol	Thickness	77.6	0.308	1.00	71.1
11.	1.5% CMC	Thickness, flow rate finite plate	31.4	0.631	1.00	66.0

EXPERIMENTS WITH NON-NEWTONIAN FLUIDS

The theory presented above was developed for a non-Newtonian fluid that may be approximated by a power law model. To check the applicability of the theory, two types of power law fluids were tested experimentally: nonelastic Carbopol solutions and viscoelastic CMC solutions. The flow behavior of Carbopol solutions has been described as inelastic (4); solutions of CMC are viscoelastic (4, 11, 13).

Carbopol solutions were selected as fluids which are closely approximated by the power law (4, 8); one report (5) indicated that they do not exhibit Newtonian behavior at low shear rates as some other non-Newtonian fluids do. Since they constituted fluids suitable to test the proposed theory, most of the runs were made with Carbopol solutions.

Properties of the non-Newtonian fluids used, together with the types of experiments performed, are listed in Table 4. Rheological measurements were made at shear stresses, in dynes per square centimeters, which ranged from 6 to 135 (for 0.16% Carbopol) to 17 to 432 (0.20% Carbopol) and to 9 to 576 (1.5% CMC). The range of shear rates for each fluid may be estimated from stresses and constants in Table 4; the gross range was from 0.007 to 260 sec.$^{-1}$.

Over these ranges of measured deformation rates and stresses all the fluids were fit by the power law to within an average of 5% or less, based on stress.

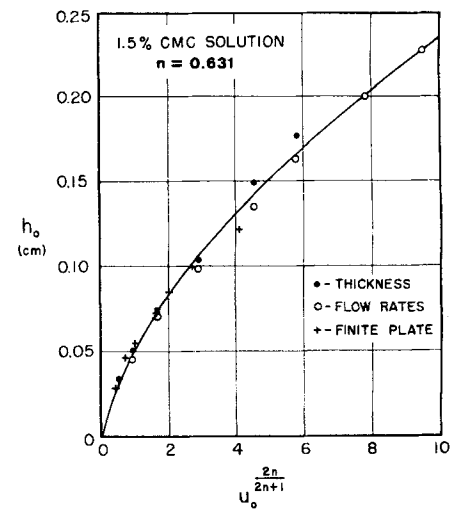

Fig. 7. Effect of withdrawal speed on film thickness—a viscoelastic fluid.

Stresses used in the rheological measurements were comparable, in general, to those encountered in the film. In no part of any film did stresses exceed the upper limit of those measured rheologically. Based on zero stress at the gas interface, Equation (21), some portions of each film had stresses below those measured rheologically. For each liquid, however, these portions comprised only about 6% of the thickness at maximum speeds. At lower speed, these portions were larger. However, since no significant deviation at low speeds was noted, as shown in Figure 6, it was concluded that the fluids were power law materials at the stresses and deformation rates encountered in the film.

The measured film thicknesses for Carbopol fluids number 7 to number 10 are plotted in Figure 6 vs. withdrawal speed raised to the power indicated by the simplified theory of Equation (41). Flow rate data for solutions having $n = 0.374$ and 0.56 are also reported as h_o in Figure 6, based on Equation (43). The good agreement of thickness and flow rate data for these fluids indicates that the theoretical interrelationship, Equation (43) in this case, is satisfactorily accurate. The straight lines in Figure 6 show that the effect of withdrawal speed predicted by Equation (41) is followed closely by Carbopol solutions over a two hundred-fold range of speed and the 0.3 to 0.6 range of n tested. As the effect of speed indicated by Equation (41) also holds for Newtonian fluids, it is believed to be applicable over the 0.3 to 1.0 range of n for power law fluids.

A solution of CMC was tested to check whether the theory could provide an approximation for the case of a viscoelastic fluid. Since the case studied involves a liquid film of an infinite thickness at the bottom contracting to a finite and small thickness h_o, it was anticipated a priori that elastic effects would have a larger influence in this case than, say, in the case of flow in closed conduits. However, the question was how much will these effects contribute and to what extent they could be tolerated. The CMC data are shown in Figure 7 on the Equation (41) type of plot used previously. The good agreement between the three types of measurements indicates the applicability of the Region 1 equations. However, the substantial deviation of the data from the straight-line relationship, predicted by the simplified theory of Equation (41), indicates that viscoelastic effects are significant under these conditions. No further analysis of CMC data was attempted.

Thickness data for the inelastic Carbopol fluids with the highest and lowest n studied are shown on $\overline{T}$ vs. N_{Ca} plots in Figures 8 and 9, together with $\overline{T}$ calculated with Equation (44) from Equations (41), (46), and (52).

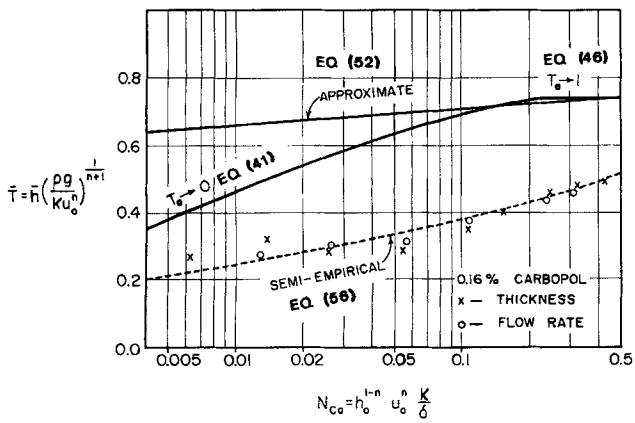

Fig. 8. Effect of capillary number on dimensionless mean thickness—power law fluid ($n = 0.56$).

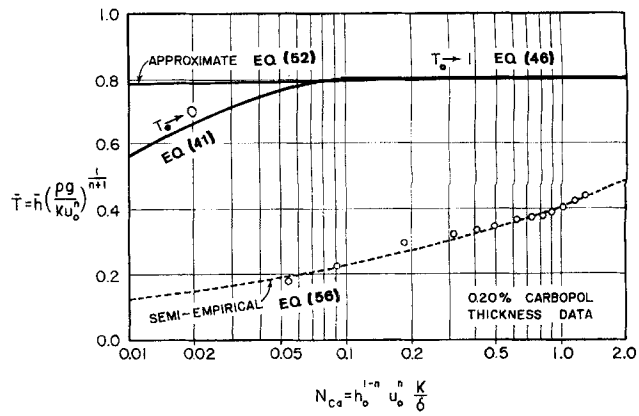

Fig. 9. Effect of capillary number on dimensionless mean thickness—power law fluid ($n = 0.308$).

As seen in these figures, the magnitude of the experimental thickness is considerably below the theoretical predictions; the theory does not agree with the data in this respect. Moreover, the disagreement becomes larger with decrease in the power law exponent n. Thus for $n = 0.56$ (0.16% Carbopol) the actual data are on the average 40% lower than the simple theory, Equations (41) and (46), and for $n = 0.308$ (0.20% Carbopol) they are 65% lower.* The difference in magnitude between Equation (52) and data is even larger than the difference between Equation (41) and data. The fact that Equation (52), which was found to correlate Newtonian data satisfactorily, does not apply in the case of power law fluids with $n < 1$ deserves further discussion.

For the two other fluids with n values between 0.308 and 0.56 the deviations are between those of the two fluids mentioned above. Thus, the theory presented here is inadequate for prediction of the absolute magnitude of film thicknesses for power law fluids.

DISCUSSION

The theory for non-Newtonian fluids only provides, in magnitude, an upper limit to $\overline{T}$ for any given capillary number; this is the same situation noted for Equation (41) for Newtonian liquids. For power law fluids however the deviations are even larger, and they increase with decreasing n. The reason for these deviations is the same as in the Newtonian case, a matching between the entrained film and the static meniscus at different, rather than equal, values of L (∞ and 1). The success of this matching depends on the rate at which the second derivatives of L attain constant values and the closeness of $L = \infty$ to $L = 1$.

This is the point where the matching assumption for non-Newtonian fluids becomes more difficult to fulfill than in the Newtonian case. To get an idea about this problem, one can compare the convergence of $d^2L/d\lambda^2$ as $L \to \infty$ for two extreme cases: $n = 1$, the Newtonian case, and $n \to 0$. Doing this, one obtains from Equation (37), upon which α and Equation (41) are based, the following:

For $n = 1$:

$$\lim_{L\to\infty} \frac{d^3L}{d\lambda^3} = \lim_{L\to\infty} \frac{L-1}{L^3} = \lim_{L\to\infty} \frac{1}{L^2} \to 0 \qquad (53)$$

For $n = 0$

$$\lim_{L\to\infty} \frac{d^3L}{d\lambda^3} = \lim_{L\to\infty} \frac{(L-1)^n}{L^{2n+1}} = \lim_{L\to\infty} \frac{1}{L} \to 0 \qquad (54)$$

* This difference is even larger on a a T_o vs. Nca plot in the vicinity of $Nca = 1$.

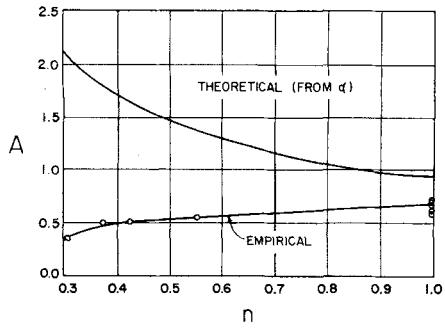

Fig. 10. Thickness coefficient A as a function of power law exponent n.

Equations (53) and (54) show that while both third derivatives converge to zero (thus assuring convergence of the second derivative to a constant), the rate of convergence is different. In the case of $n = 0$, the convergence is considerably slower. Therefore, at values of n less than 1, the second derivative becomes constant only at a higher L; the value of the constant α is higher, and as a result estimates for T_o and $\overline{T}$ will be higher than for $n = 1.0$.

The case of the approximate solution, Equation (52), is even worse as shown by examining Equation (51), upon which β is based. When one uses Equation (51), the limit for $n = 1$ remains the same as in Equation (53). However, for $n \to 0$

$$\lim_{L\to\infty} \frac{d^3L}{d\chi^3} = \lim_{L\to\infty} \frac{L-1}{L^{2n+1}} = \lim_{L\to\infty} \frac{L}{L} = 1 \qquad (55)$$

Since the third derivative, for $n \to 0$, does not vanish in the limit as $L \to \infty$, the second derivative does not converge at all. Although for cases of n larger than zero the second derivative does converge, the convergence is very slow and the constant β is much higher. This conclusion is illustrated by comparison of the respective values of α and β in Tables 1 and 2. Thus one may conclude that Equation (52) will probably fit only in the neighborhood of $n = 1$, say $n > 0.8$, but will give erroneous results for lower n's.

This problem resembles somewhat the case of boundary-layer assumptions in power law fluids (6), where the assumptions are also harder to fulfill than in the Newtonian case.

SEMIEMPIRICAL RELATIONSHIP

The functional relationship between h_o, u_o, and fluid properties, described in Equations (40) and (41), is based on matching of solutions, Equation (35), and on α from Equation (36). This matching of solutions, done at two different L's (1 and ∞), does not predict the absolute magnitude of $\overline{T}$ found experimentally. On the other hand, the functional form of Equation (41) does predict the relationship between h_o and velocity over a two hundred-fold range of velocity; this has been shown for various fluids in Figures 4 and 6. Thus, only the coefficient α seems to be in error.

In order to predict the proper coefficient, matching at equal values of L was considered in place of matching in accordance with Equation (35). It was found that instead of separable solutions for both derivatives at values which were only functions of n, the interrelating matching equation was not separable. Thus, integrations involving specified values of T_o and N_{Ca} as well as n were required (integrations over three dimensions rather than one dimension) from which discrete pairs of T_o and N_{Ca} at given n are obtainable only by iteration. From preliminary calculations, it was clear that resultant values of α would be functions of N_{Ca} as well as n.

During preliminary calculations for matching at equal L's it was noted that at the high L values required for matching, two assumptions implied in the dynamic meniscus Equation (18) are questionable: namely one-dimensional flow and use of d^3h/dx^3 as the approximate surface tension term [in place of the exact expression, which is the x derivative of the left side of Equation (19)]. The uncertainties and inaccuracies due to these assumptions in the range of required calculations and the more complex α dependence which would result led the authors to the following semiempirical approach.

The general relationship for all data was developed from functional forms predicted by theory, that is Equations (40) and (41), and a numerical coefficient α_{exp} determined empirically. Values of α_{exp} were calculated from the slopes of the straight lines in Figure 4 and 6.

This relationship may be expressed either in dimensionless form (T_o or $\overline{T}$ and N_{Ca}) or in dimensional form (with h_o, u_o, and fluid properties). Although a relationship between T_o and $\overline{T}$ and N_{Ca} is convenient for comparing theory and experiment, it is not convenient for practical purposes. This is due to the fact that in the case of non-Newtonian fluids both T_o and N_{Ca} contain the dependent variable h_o, as opposed to the Newtonian case, where only T_o contains h_o.

Thus, a dimensional relationship is preferred in order to obtain an expression explicit in film thickness.

Using Equation (40), modified by substituting α_{exp}, a coefficient determined experimentally, one arrives at

$$h_o = \left[\left(\frac{2n+1}{n} \right)^{2n} \left(\frac{\alpha_{exp}}{\sqrt{2}} \right)^3 \right]^{1/(2n+1)} \left(\frac{K^2 u_o^{2n}}{\sqrt{\sigma}(\rho g)^{3/2}} \right)^{1/(2n+1)} \qquad (56a)$$

Since α_{exp} is a function of n only, Equation (56a) may be rewritten by introducing a new empirical constant $A = A(n)$ as follows:

$$h_o = A \left[\frac{K^2 u_o^{2n}}{\sqrt{\sigma}(\rho g)^{3/2}} \right]^{1/(2n+1)} \qquad (56b)$$

Values of the empirical coefficient A as a function of n are shown in Figure 10 together with theoretical values of A calculated from α given in Table 1. The difference between the two values of A, shown in Figure 10, repre-

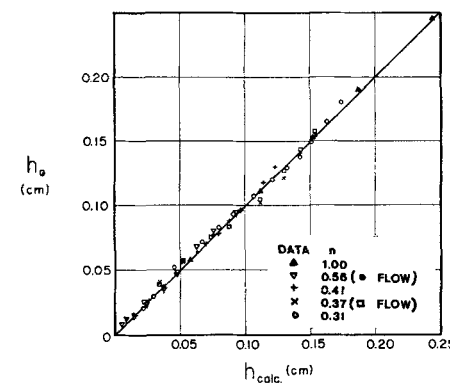

Fig. 11. Comparison between measured thickness h_o and that calculated from the semiempirical equation.

sents the magnitude of the deviation between theory and experiment in terms of film thickness h_o.

Equation (56) together with A values shown in Figure 10 represents an equation for film thickness which holds both for Newtonian and inelastic power law fluids. This is the general relationship. Values of $\overline{T}$ from Equation (56) and Figure 10, plotted in Figures 8 and 9 as dashed lines, indicate good agreement with individual runs at $n = 0.308$ and $n = 0.56$. A more complete indication of the good agreement of individual runs with Equation (56) is shown in Figure 11, which includes all the thickness and flow rate data obtained with Carbopol solutions and data from one Newtonian fluid.

It is worthwhile examining how well withdrawal is described by simple drainage theory for two reasons: first, since the semiempirical withdrawal Equation (56) indicates that film thickness is relatively insensitive to changes in surface tension, and second, since drainage equations, which were based on negligible surface tension, are easier to derive than withdrawal equations, which include surface tension effects. This examination was done by comparison of Equations (45) to (47) based on drainage with Equations (41) to (44) and (56) based on withdrawal.

Comparison of the magnitude of film thickness, as shown in Figures 8 and 9 by comparing withdrawal Equation (56) with drainage Equation (46), indicates that drainage theory describes an upper limit on withdrawal thickness; this upper limit was not exceeded at any withdrawal speed or fluid property studied. Furthermore, the five conclusions regarding the effect of n, described after drainage Equation (16), are equally valid for withdrawal without any modification. Comparison of drainage Equation (45) with withdrawal Equation (56) indicates that the effects of u_o, K, and ρ for given n, are slightly different.

Based on these comparisons, it was concluded that drainage theory is a useful first approximation for the withdrawal case, both for estimating the thickness dependence on speed and all fluid properties except surface tension and the order of magnitude and maximum size of the film thickness and flux. Therefore, it is believed that drainage provides a useful basis for estimating withdrawal conditions where withdrawal theories or results are not available.

SUMMARY

1. A theory of drainage and withdrawal of liquid films of non-Newtonian fluids was developed for flat plates. The drainage case was solved for an Ellis model, the withdrawal case for a power law fluid.

2. Withdrawal experiments were performed with Newtonian and power law fluids. Data for n ranging from 0.3 to 1.0 were obtained over a two hundred-fold range of withdrawal speeds. In addition, the simple power law model was tested experimentally on a viscoelastic fluid.

3. The functional relationship for the withdrawal case, Equation (40), was confirmed by experiments for simple power law fluids. However, the absolute magnitude of the film thickness predicted by theory was about twice that found by experiment.

4. An approximate solution, Equation (52) which correlated Newtonian experiments satisfactorily in other work, did not hold for power law fluids.

5. A semiempirical relationship was developed for withdrawal, Equation (56); this equation satisfactorily correlated film thicknesses for power law fluids having n values from 0.3 to 1.0.

6. Experimental evidence for a viscoelastic fluid indicates that elastic effects have a much larger influence in withdrawal than in the case of flow in closed conduits. Data were not correlated satisfactorily by the present theory.

ACKNOWLEDGMENT

The authors are grateful for the National Science Foundation Grant 19820 by which this work was supported and for the support of the Yale Computer Center.

NOTATION

A = a constant defined by Equation (56)
a = rheological constant, Equation (5)
b = rheological constant, Equation (5)
d = immersion depth of finite plate
g = gravitational acceleration
h = film thickness at any point
h_o = film thickness at top of the dynamic meniscus
$\overline{h}$ = mean film thickness $= Q/u_o$ [also defined by Equation (11)]
i = summation index
K = rheological constant, consistency index, Equation (13)
L = dimensionless coordinate (h/h_o)
n = rheological constant, power law exponent, Equation (13)
N_{Ca} = capillary number $= h^{1-n}u_o{}^nK/\sigma$
Q = flux, volume flow rate per unit width
s = rheological constant, Equation (5)
t = time
T = dimensionless thickness $= h\left(\frac{\rho g}{Ku_o{}^n}\right)^{1/(n+1)}$
$\overline{T},T_o$ = dimensionless thickness for $\overline{h}$ and h_o
u = velocity in the plate direction
u_o = velocity of solid support
u_h = velocity at the air liquid interface
x,y = coordinates

Greek Letters

α = constant defined by Equation (36)
α_{exp} = constant defined by Equation (56a)
β = constant $= \left(\frac{d^2L}{d\chi^2}\right)_{L\to\infty}$
Δ = integration step
ϵ = small number
λ = dimensionless coordinate defined by Equation (29)
μ = viscosity (Newtonian)
ρ = density
σ = surface tension at the liquid-air interface
τ_{xy} = xy component of the stress tensor
χ = dimensionless coordinate defined by Equation (50)

Note: All dimensional quantities are in C.G.S. units

LITERATURE CITED

1. Blok, H., "Societe Belge pour l'etude du petrole," Brussels (Feb., 1946).
2. Deryagin, B. V., *Dokol. Akad. Nauk. S.S.S.R.*, **39**, 13 (1943).
3. ———, and A. S. Titiyevskaya, *ibid.*, **50**, 307 (1945).
4. Dodge, D. W., and A. B. Metzner, *A.I.Ch.E. Journal*, **5**, 189 (1959).
5. Fisher, W. H., W. H. Bauer, and S. E. Wiberly, *Trans. Soc. Rheol.*, **5**, 221 (1961).
6. Gutfinger, Chaim, and R. Shinnar, *A.I.Ch.E. Journal*, **10**, 631 (1964).

7. ———, and J. A. Tallmadge, *ibid.*, 744.
8. ———, Ph.D. thesis, Yale Univ., New Haven, Connecticut (August, 1964).
9. Jeffreys, H., *Proc. Camb. Phil. Soc.*, **26**, 204 (1930).
10. Levich, V. G., "Physicochemical Hydrodynamics," Chap. 12, Prentice Hall, Englewood Cliffs, New Jersey (1962).
11. Metzner, A. B., W. T. Houghton, R. A. Sailor, and J. L. White, *Trans. Soc. Rheol.*, **5**, 133 (1961).
12. Morey, F. C., *J. Research, U. S. Natl. Bur. Stands.*, **25**, 385 (1940).
13. Philippoff, W., in "Progress in International Research on Thermodynamic and Transport Properties," pp. 698-703, Academic Press, New York (1962).
14. Satterly, J., and G. Givens, *Trans. Roy Soc. Canada*, **27**, 145 (1933).
15. Van Rossum, J. J., *Appl. Sci. Res.*, **A7**, 121 (1958).
16. White, D. A., and J. A. Tallmadge, *Chem. Eng. Sci.*, **20**, 33 (1965).

Manuscript received July 23, 1964; revision received October 15, 1964; paper accepted October 23, 1964. Paper presented at A.I.Ch.E. Boston meeting.

Coalescence of Liquid Droplets in Two-Component—Two-Phase Systems:

Part I. Effect of Physical Properties on the Rate of Coalescence

G. V. JEFFREYS and J. L. HAWKSLEY

The Manchester College of Science and Technology, Manchester, England

Experimental coalescence time and time distribution studies of the coalescence of a single droplet at a plane interface are presented for four two-component–two-phase systems. The results have been analyzed by dimensional analysis and statistical analysis, and a correlation of coalescence time and coalescence time distribution with the physical properties of the system is proposed.

The coalescence of liquid dispersions is of great interest in many scientific fields, particularly in solvent extraction equipment where the generation of secondary mists result in entrainment and loss of efficiency. Therefore it is very important that the mechanism of the coalescence process is understood and that the effects of the physical properties of the participating phases on the rate of coalescence can be assessed.

Notable contributions to the understanding of coalescence mechanism have been made by Cockbain and Roberts (*1*), Elton and Picknett (*2*), Gillespie and Rideal (*3*), and many others. Also in recent years the studies by Charles and Mason (*4*) and Mackay and Mason (*5*) on the rate of thinning of the film between the droplet and the interface, and the work of Lang (*6*) on the effects of vibrations on this film, have resulted in proposals for the prediction of the rate of coalescence of single droplets at an interface in two-component–two-phase systems. The equations derived by these workers have been developed from the Navier-Stokes equation which specifies the physical properties of the phases and their significance in the systems to be studied. Furthermore the analysis was applied to drop-interface arrangements of specific geometry. Hence it would be very interesting to investigate the significance of all the possible physical properties of the system on the rate of coalescence, and the following paper presents the results of such a study. The investigation was initiated by a dimensional analysis of the problem, and the results of this analysis were further considered by a statistical analysis of a factorial experiment of the coalescence process. These aspects of the study are described, and a correlation relating coalescence time with the physical properties of the system is presented. This is followed in Part II with a description of high speed photographic work undertaken, and the flow characteristics of the film between the drop and interface are analyzed. This analysis has been applied to droplet-interface geometries obtained from the photographic studies in order to predict the pressure in the film at the mid point vertical axis and to compare it with the pressure inside the droplet in order to confirm the shape of droplets resting on an interface and explain the distribution of coalescence time results reported by all experimenters in this field.

EXPERIMENTAL APPARATUS

The all glass coalescence apparatus is shown in Figure 1 and was developed from that used in a previous investigation

J. L. Hawksley is with Imperial Chemical Industries, Ltd., Billingham, England.